




Letter

Coexistence of low- K oblate and high- K prolate $g_{9/2}$ proton-hole bands in ^{115}Sb

Shabir Dar ^{a,b}, S. Bhattacharyya ^{a,b}, *, S. Chakraborty ^a, S. Jehangir ^c, Soumik Bhattacharya ^a, G.H. Bhat ^d, J.A. Sheikh ^e, N. Rather ^c, S.S. Nayak ^{a,b}, Sneha Das ^{a,b}, S. Basu ^{a,b}, G. Mukherjee ^{a,b}, S. Nandi ^{a,b,1}, R. Banik ^f, S. Basak ^{a,b}, C. Bhattacharya ^{a,b}, S. Chattopadhyay ^{g,b}, S. Das Gupta ^h, A. Karmakar ^{g,b}, S.S. Ghugre ⁱ, D. Kumar ^{a,b}, D. Mondal ^a, S. Mukhopadhyay ^{a,b}, D. Pandit ^a, S. Rajbanshi ^j, R. Raut ⁱ

^a Variable Energy Cyclotron Centre, Kolkata, 700064, India

^b Homi Bhabha National Institute, Mumbai, 400094, India

^c Department of Physics, Islamic University of Science and Technology, Awantipora, 192122, India

^d Department of Physics, Sri Pratap College, Srinagar, 190001, India

^e Department of Physics, University of Kashmir, Srinagar, 190006, India

^f Institute of Engineering and Management, Kolkata, 700091, India

^g Saha Institute of Nuclear Physics, Kolkata, 700064, India

^h Victoria Institution (College), Kolkata, 700009, India

ⁱ UGC-DAE Consortium for Scientific Research, Kolkata Centre, Kolkata, 700098, India

^j Department of Physics, Presidency University, Kolkata, 700073, India

ARTICLE INFO

Editor: B. Blank

Keywords:

Shape coexistence

Low- K

High- K

INGA

PSM

ABSTRACT

A positive parity sequence of $\Delta I = 2$ γ transitions has been identified above $I^\pi = 9/2^+$ state ($E_x = 2019$ keV) in ^{115}Sb through in-beam γ ray spectroscopic technique. Rotational features of this sequence are found similar to a low- K decoupled band. Observation of this newly identified low- K decoupled band, along with the earlier reported strongly coupled high- K band in this nucleus, provides the first experimental evidence for prolate-oblate shape coexistence associated with $g_{9/2}$ proton-hole configuration around $Z = 50$ shell closure. Experimental results are reproduced reasonably well in the frameworks of the projected shell model and the total Routhian surface calculations.

As a many-body quantal system, atomic nuclei are excellent laboratories for testing various quantum mechanical phenomena. The shape coexistence in the realm of atomic nuclei has long been a topic of interest as its exploration across the Segrè chart can provide insight into the underlying nucleonic shell structures. The phenomenon of nuclear shape coexistence was started with the observation of the deformed $I^\pi = 0_2^+$ state in the doubly magic ^{16}O nucleus along with the spherical $I^\pi = 0_1^+$ ground state [1–3]. Thereafter, such coexistence of spherical and deformed shapes were also identified near different shell closures across the nuclear landscape [4–6]. The best evidence to date for a coexistence of the states corresponding to prolate, oblate and spherical shapes at low excitation energy was found in ^{186}Pb [7].

The nuclei in $A \approx 110 - 120$ region mainly exhibit weak deformation at lower angular momentum with the observation of non-collective single-particle excitations. Of special interest in this region of the Segrè chart, lying close to the $Z = 50$ shell closure, is the observation of rotational bands associated with the shape-driving high- j orbitals. Most of these deformed rotational bands have elongated cigar-like prolate deformation. The particle-hole excitations across the $Z = 50$ closed shell play a dominant role to develop the deformation in these nuclei. Consequently, coexistence of the collective and non-collective structures was reported in several even-even, odd- A and odd-odd nuclei in this mass region [8–18]. In addition, shape transition from collective prolate to non-collective oblate over a range of angular momentum and excita-

* Corresponding author at: Variable Energy Cyclotron Centre, Kolkata, 700064, India.

E-mail address: sarmi@vecc.gov.in (S. Bhattacharyya).

¹ Presently at: Subatech (IMT Atlantique, CNRS/IN2P3, Nantes Universite), 4 rue Alfred Kastler, 44307 Nantes cedex 3, France.

<https://doi.org/10.1016/j.physletb.2024.138565>

Received 19 June 2023; Received in revised form 21 February 2024; Accepted 4 March 2024

Available online 7 March 2024

0370-2693/© 2024 The Author(s). Published by Elsevier B.V. Funded by SCOAP³. This is an open access article under the CC BY license (<http://creativecommons.org/licenses/by/4.0/>).

tion energy was also reported in a few nuclei, such as, odd-A $^{115-121}\text{I}$ [19–23] and $^{121,122}\text{Xe}$ [24,25]. However, the coexistence of two or more distinctive deformed shapes in a narrow range of energy and angular momentum is not found to occur very often. Limited observations of collective prolate-oblate shape coexistence were reported in odd-A $^{119-121}\text{I}$ [22,26] and ^{119}Cs [27] nuclei associated with the unique parity $\pi h_{11/2}$ configuration. In this context, it may be noted that, the Antimony isotopes ($Z = 51$), with an odd quasi-proton above the $Z = 50$ shell closure, have two shape driving high- j orbitals, viz, $g_{9/2}$ and $h_{11/2}$, near the proton Fermi surface. The general tendency that these orbitals can induce prolate and oblate shapes is also evident from the Nilsson diagrams. Consequently, a prolate deformed strongly coupled $\Delta I = 1$ rotational band based on a $\pi[404]_{9/2}^{-}$ high- K configuration was observed systematically in the odd-A Sb isotopes [11,13]. Despite the fact that, competition between the prolate and oblate shapes is likely at the top of the $g_{9/2}$ orbital, the rotational band based on the same orbital with oblate deformation has not yet been observed in this mass region. In nature oblate shapes occur rarely as compared to more frequent prolate shapes. The explanation to this tendency of strong dominance of prolate shapes over the oblate has not been resolved fully and needs more experimental investigations. This letter reports the first observation of oblate deformed decoupled $\Delta I = 2$ rotational band associated with a $\pi[440]_{1/2}^{-}$ low- K configuration, along with the known high- K prolate deformed band in ^{115}Sb . This is so far the only instance where coexisting prolate and oblate deformed bands, based on $\pi g_{9/2}^{-1}$ orbital, are observed in any of the $Z > 50$ nuclei.

The excited states in ^{115}Sb were populated via $^{115}\text{In}(^4\text{He}, 4n\gamma)$ fusion-evaporation reaction at a beam energy of $E_\alpha = 52$ MeV, obtained from the K-130 Cyclotron at Variable Energy Cyclotron Centre (VECC), Kolkata, India. A 20 mg/cm² thick self-supporting foil of natural Indium was used as the target. Eleven Compton suppressed Clover HPGe detectors, mounted in the modified support structure of the Indian National Gamma Array (INGA), were used to detect the de-exciting γ -rays. Six of these detectors were placed at $\theta = 90^\circ$ ($\phi = 0^\circ, 36^\circ, 72^\circ, 108^\circ, 144^\circ, 180^\circ$), three at $\theta = 125^\circ$ ($\phi = 0^\circ, 90^\circ, 180^\circ$) and two at $\theta = 40^\circ$ ($\phi = 0^\circ, 90^\circ$) with respect to the beam direction. A Pixie-16 digitizer based pulse processing and data acquisition system was employed to record the valid γ events in singles and coincidence mode [28]. Standard ^{152}Eu and ^{133}Ba radioactive γ sources were utilised for energy and efficiency calibrations.

The offline sorting of gain-matched raw data was carried out using BiNDAS [29] and IUCPIX [28] software packages. A symmetric E_γ - E_γ matrix and E_γ - E_γ - E_γ cube were formed from the add-backs of all the clover detectors to establish the coincidence relations between the de-exciting γ rays. An asymmetric matrix with events recorded at $\theta = 90^\circ$ along one axis and those at $\theta = 125^\circ$ along the other was used to deduce the multiplicities of the de-exciting γ rays using the method of Directional Correlation from Oriented states (DCO) [30]. Two other matrices formed from the detectors at $\theta = 90^\circ$ were used to determine the electric or magnetic character (E/M) of the γ rays by Polarization Directional Correlation from Oriented states (PDCO) method [31–33]. These matrices correspond to the events recorded in the segments of the clover detector, which are perpendicular and parallel to the emission plane, in coincidence with events recorded in all the other detectors of the setup. These measurements were subsequently used to build the level scheme and also to assign the spin and parity of the excited energy levels. The offline data analysis was carried out using the Radware suite of packages [34]. Details of the data analysis procedures are available in Ref. [35].

The partial level scheme of ^{115}Sb , as shown in the Fig. 1, is developed in the present work on the basis of γ ray coincidence and intensity relationships. The excited levels are grouped mainly into two bands: 1 and 2. The band 1, with $I^\pi = 9/2^+$ at $E_{\text{level}} = 1380$ keV as the band-head, was reported earlier upto $I^\pi = 37/2^+$ [36]. In this work, all the γ rays and excited states of band 1 upto $I^\pi = 35/2^+$ were observed and found unaltered. A new cascade of four γ transitions, marked as 2

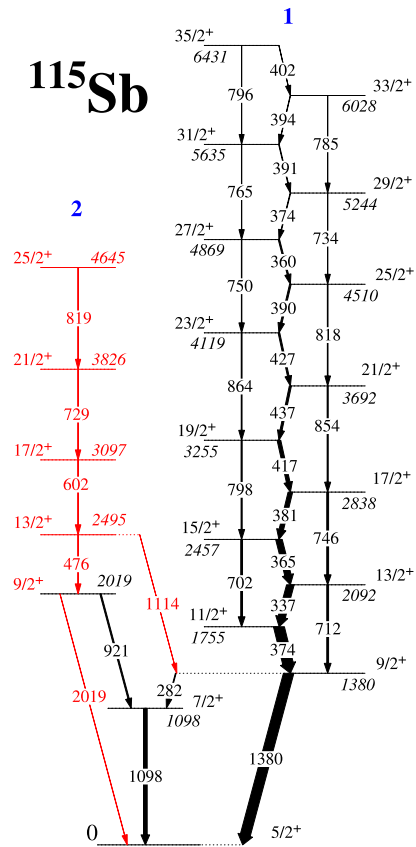


Fig. 1. The $\pi g_{9/2}^{-1}$ bands in ^{115}Sb . New experimental information are marked in the red colour.

in Fig. 1, was identified in the present work. Fig. 2 represents double-gated coincidence spectra with gates on: (a) 1380 & 374 keV and (b) 1098 & 921 keV transitions corresponding to the bands 1 and 2, respectively, whereas, (c) 602 & 729 keV corresponding to their connection via 1114 keV transition. The inset in the spectrum of Fig. 2 (a) shows the crossover E2 transitions corresponding to band 1. Observation of all the four γ rays, viz, 476, 602, 729 and 819 keV, in the 1098 and 921 keV double-gated spectrum (Fig. 2 (b)) provide support in favour of their placements in band 2. The band 2 is found to decay to the ground state mainly via a cascade of 921 and 1098 keV γ rays and also through the newly observed 2019 keV and 1114 keV γ transitions. Spins and parities of all the states were assigned unambiguously from the present spectroscopic results, as summarised in Table 1.

In the $A \approx 110 - 120$ region, the proton Fermi surface lies near the prolate driving low- K $h_{11/2}$ and high- K $g_{9/2}$ high- j orbitals [37]. Accordingly, a decoupled (strongly coupled) band associated with the $\pi h_{11/2}$ ($\pi g_{9/2}^{-1}$) configuration was reported systematically in odd-A Sb, I and Cs isotopes in this region [13,20,27,36,38–41]. On the other hand, the high- K $h_{11/2}$ and low- K $g_{9/2}$ orbitals are also available near the proton Fermi surface with oblate deformation. As a consequence, a strongly coupled negative parity band was reported in $^{119,121}\text{I}$ [22,26] and ^{119}Cs [27]. This provides an evidence of prolate-oblate shape coexistence based on $\pi h_{11/2}$ orbitals. However, the band based on an oblate deformed low- K $\pi g_{9/2}^{-1}$ orbital is hitherto unreported in this mass region. The newly observed band 2 in ^{115}Sb is found to exhibit a decoupled nature. Thus, it may serve as the first observation of the collective oblate band based on the low- K $\pi g_{9/2}^{-1}$ orbital in this region.

The aligned angular momentum (i_x) is plotted as a function of rotational frequency ($\hbar\omega$) in Fig. 3. It depicts larger values for band 2 compared to band 1 in ^{115}Sb at low rotational frequencies. Also, it is noted from the figure that the plots look very similar for the two iso-

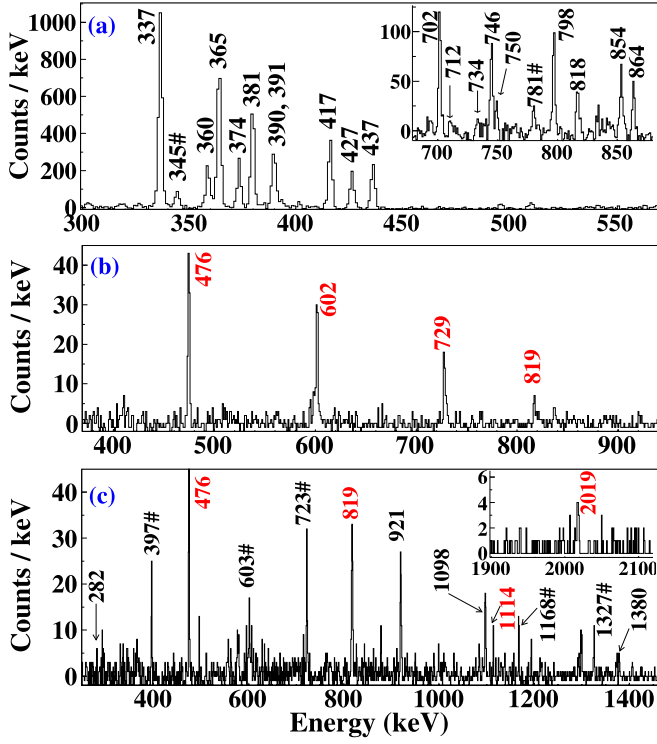


Fig. 2. Coincidence spectra corresponding to the double gates of: (a) 1380 & 374 keV (band 1), (b) 1098 & 921 keV (band 2) and (c) 602 & 729 keV transitions from E γ -E γ -E γ cube. The insets of spectra (a) and (c) correspond to crossover E2 transitions of band 1 and the decay of 9/2⁺ state of band 2 to 5/2⁺ ground state via 2019 keV transition, respectively. The red marked transitions in the spectrum (b) and (c) are newly observed in the present work, whereas, the # marked transitions in the spectra are the transitions not shown in the partial level scheme of ¹¹⁵Sb.

Table 1

The table contains the energies (E_γ), relative intensities (I_γ), experimental DCO ratios (R_{DCO}) obtained in stretched quadrupole gate and linear polarization asymmetry (Δ_{PDCO}) of the newly observed γ transitions in ¹¹⁵Sb along with the spin and parity of the initial and final states. The relative intensities are normalized to the known 1300 keV transition ($I_\gamma(1300 \text{ keV}) = 100$) in ¹¹⁵Sb, not shown in the partial level scheme. The quoted uncertainties are purely statistical, however, the additional uncertainty of 3–5% due to efficiency of the setup may be considered, depending upon the intensity of the gamma rays.

E_γ (keV)	$J_i^\pi \rightarrow J_f^\pi$	I_γ (Err)	R_{DCO} (Err)	Δ_{PDCO} (Err)
475.5(1)	13/2 ⁺ \rightarrow 9/2 ⁺	1.94(1)	1.03(2)	0.13(1)
602.2(1)	17/2 ⁺ \rightarrow 13/2 ⁺	1.61(2)	1.07(6)	0.09(2)
729.0(1)	21/2 ⁺ \rightarrow 17/2 ⁺	1.13(1)	1.02(6)	0.05(2)
818.6(2)	25/2 ⁺ \rightarrow 21/2 ⁺	0.57(3)	1.06(4)	0.19(5)
1114.4(3)	13/2 ⁺ \rightarrow 9/2 ⁺	0.35(1)	0.94(8)	0.05(7)
2019.0(2)	9/2 ⁺ \rightarrow 5/2 ⁺	0.7(1)	0.94(6)	0.06(3)

topes ^{115,117}Sb in the configuration of a $g_{7/2}$ proton coupled to the 2p-2h states in the neighbouring even-even nuclei. However, both are different from that of band 2 in ¹¹⁵Sb, which has slightly a higher alignment. This indicates that the band 2 in ¹¹⁵Sb is based on a configuration of an odd proton in low- K orbital. Together with the positive parity of this band, it suggests that the band 2 in ¹¹⁵Sb is based on a $g_{9/2}$ orbital with an oblate deformation.

Further, theoretical calculations have been carried out under the frameworks of the total routhian surface (TRS) and the projected shell model (PSM) to explore the microscopic structure of these bands in ¹¹⁵Sb and are discussed in the following.

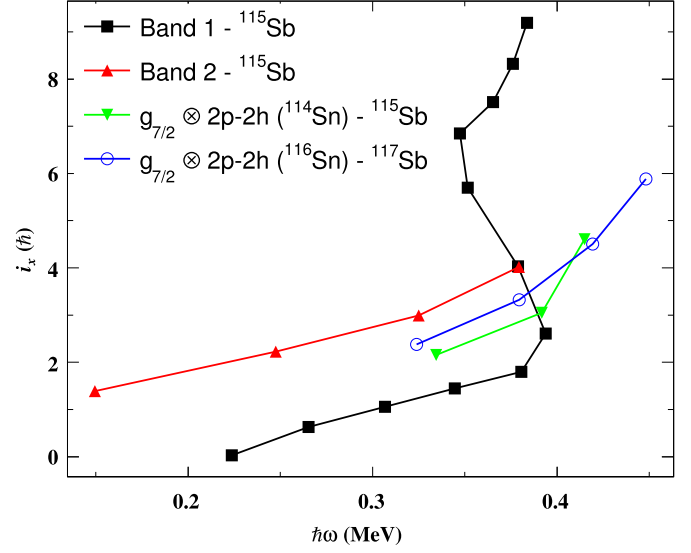


Fig. 3. Plot of aligned angular momentum (i_x) as a function of rotational frequency ($\hbar\omega$) for different bands of ¹¹⁵Sb and ¹¹⁷Sb. The Harris parameters used are $J_0 = 17 \hbar^2 \text{ MeV}^{-1}$ and $J_1 = 12 \hbar^4 \text{ MeV}^{-3}$. Data for $g_{7/2}$ bands are taken from ref. [39] for ¹¹⁷Sb and ref. [42] for ¹¹⁵Sb.

Total routhian surface calculation

The TRS calculations have been performed for the 3-quasiparticle (qp) positive parity configuration of ¹¹⁵Sb with $(\beta_2, \gamma, \beta_4)$ mesh points (where β_2 and β_4 are quadrupole and hexadecapole deformation parameters and $\gamma = 0^\circ (\pm 60^\circ)$ corresponds to prolate (oblate) shape in the Lund convention) using Nilsson-Strutinsky formalism with Woods-Saxon potential [43,44]. The TRSs are plotted in the (β_2, γ) contours after minimization on β_4 . The calculations are performed at different frequencies ($\hbar\omega$) and the (β_2, γ) values corresponding to the minimum of the TRSs are considered as the shape of the nucleus for that frequency, as outlined in Ref. [45]. The TRS calculations have been successfully used to understand the structure of nuclei in different mass regions [46–48] of the periodic table.

The TRS plots calculated for $\hbar\omega = 0.1 \text{ MeV}$ and 0.35 MeV for the positive parity bands in ¹¹⁵Sb are shown in Fig. 4. Two minima with one close to the prolate and another to oblate shape are obtained at higher frequency. The fact that the energy of the oblate minimum is about a MeV higher, corroborates well with the observation in Fig. 1 that the band 2 lies at about 640 keV above the band 1.

Projected shell model analysis

The theoretical study using PSM approach [49,50] has also been employed to discern the microscopic structures of bands observed in ¹¹⁵Sb nucleus. It is known that PSM provides an excellent and unified description of low- as well as high-spin properties of deformed nuclei [49–54]. PSM is essentially a shell-model truncation scheme with deformed basis and angular momentum projected deformed basis is employed to diagonalize the shell model Hamiltonian [55,56]. The Hamiltonian consists of a sum of schematic (i.e. quadrupole-quadrupole (QQ) + monopole pairing + quadrupole pairing) forces, which takes the form

$$\hat{H} = \hat{H}_0 - \frac{1}{2} \chi \sum_{\mu} \hat{Q}_{\mu}^{\dagger} \hat{Q}_{\mu} - G_M \hat{P}^{\dagger} \hat{P} - G_Q \sum_{\mu} \hat{P}_{\mu}^{\dagger} \hat{P}_{\mu}, \quad (1)$$

\hat{H}_0 in the above equation is the spherical single-particle potential [57]. The quadrupole \hat{Q}_{μ} , the monopole-pairing \hat{P} , and the quadrupole-pairing \hat{P}_{μ} operators are given by

$$\hat{Q}_{\mu} = \sum_{k,l} (\hat{Q}_{\mu})_{k,l} c_k^{\dagger} c_l, \quad \hat{P} = \frac{1}{2} \sum_k c_k c_k, \quad \hat{P}_{\mu} = \frac{1}{2} \sum_{k,l} (Q_{\mu})_{kl} c_k c_l,$$

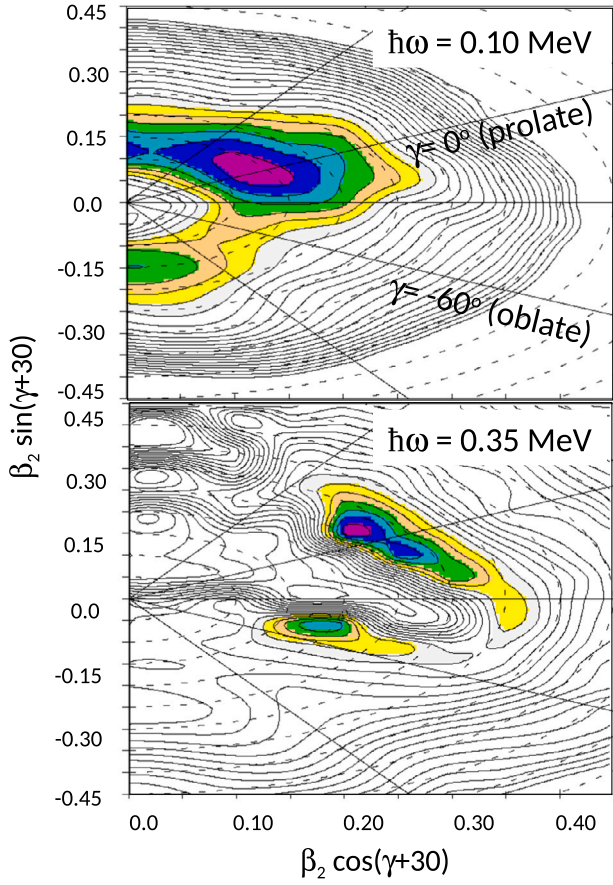


Fig. 4. TRS plot for ^{115}Sb at two rotational frequencies ($\hbar\omega$), calculated for the positive parity configuration. The contours are 400 keV apart.

with $\hat{Q}_\mu = r^2 Y_{2\mu}$. The strength of the quadrupole force χ is adjusted such that the known quadrupole deformation parameters ϵ are obtained [58] as a result of the Hartree-Fock-Bogoliubov self-consistent procedure. The monopole-pairing-force constants G_M are chosen such that the overall observed odd-even mass differences are reproduced in the given mass region and are of the standard form

$$G_M = \frac{G_1 - G_2 \frac{N-Z}{A}}{A} \text{ for neutrons, } G_M = \frac{G_1}{A} \text{ for protons.} \quad (2)$$

In the present calculation, we take $G_1 = 20.12$ and $G_2 = 13.13$. This choice of G_M is appropriate for the single-particle space employed in the model, where three major shells are used for each type of nucleons $N = (3, 4, 5)$ for both neutrons and protons. The strength parameter G_Q for quadrupole pairing is simply taken to be proportional to G_M . The proportionality constant varies slightly from nucleus to nucleus as to reproduce the band crossing at the right place; in the present calculation, on the average, it turns out to be around 0.18.

In the present study of ^{115}Sb nucleus (odd-proton system), PSM model space is composed of (angular-momentum-projected) of one- and three-qp basis, i.e.,

$$\{ |\Phi\rangle \} = \{ a_\pi^\dagger |\Phi\rangle; a_\pi^\dagger a_{v_1}^\dagger a_{v_2}^\dagger |\Phi\rangle \}, \quad (3)$$

where the three-dimensional angular-momentum operator is [59]

$$\hat{P}_{MK}^I = \frac{2I+1}{8\pi^2} \int d\Omega D_{MK}^I(\Omega) \hat{R}(\Omega), \quad (4)$$

with

$$\hat{R}(\Omega) = e^{-i\alpha \hat{J}_z} e^{-i\beta \hat{J}_y} e^{-i\gamma \hat{J}_z}, \quad (5)$$

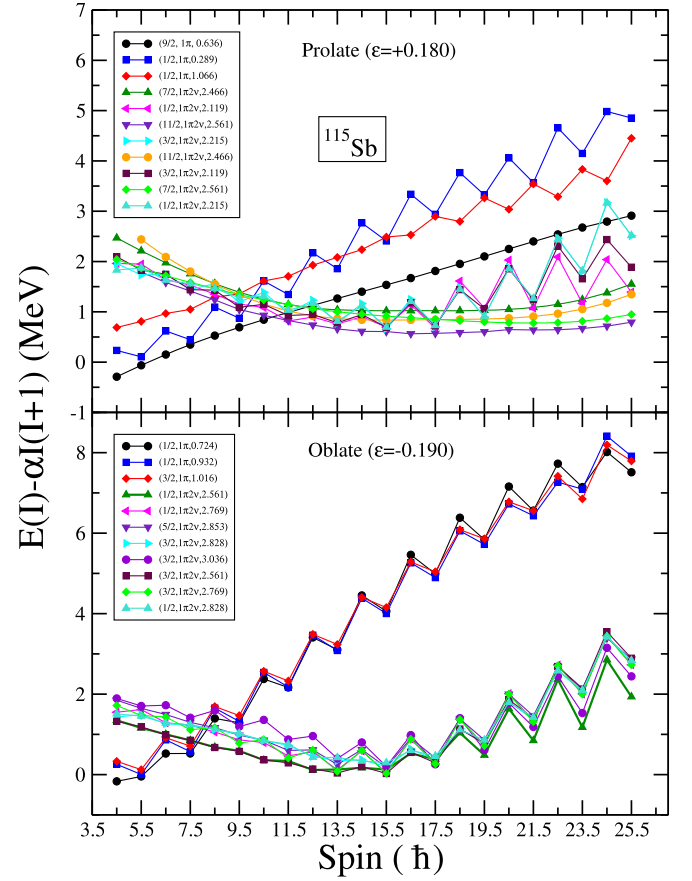


Fig. 5. Projected energies are shown before diagonalization of the shell model Hamiltonian for ^{115}Sb . Only the lowest few bands are labelled by three quantities: K-quantum number, group structure and energy of the quasiparticle state. For instance, $(9/2, 1\pi, 0.63)$ designates one-quasiproton state having intrinsic energy of 0.63 MeV and $K = 9/2$.

and $|\Phi\rangle$ represents the qp vacuum state. To investigate the possibility that two band structures observed in ^{115}Sb corresponding to prolate and oblate shapes, we have performed two sets of PSM calculations - one with the prolate deformation of $\beta = +0.18$ and the other with the oblate deformation of $\beta = -0.19$. For each of these sets, several intrinsic states in the vicinity of the Fermi surface are chosen and are projected to good angular-momentum states. The energy versus angular-momentum plot, what is referred to as the band diagram, is depicted in Fig. 5. The ground-state band for the prolate shape corresponds to the projected band from the intrinsic one quasiproton configuration with $K = 9/2$. This band is then crossed by three quasiparticle configuration with $K = 11/2$. For the oblate shape, it is evident from the band diagram that the lowest band structure originates from low-K values.

The projected bands depicted in Fig. 5 and many other projected states from the quasiparticle configurations close to the Fermi surface are used to diagonalize the shell model Hamiltonian (Eqn. (1)) separately for prolate and oblate shapes. The lowest energies obtained after configuration mixing for both prolate and oblate deformations are compared with the corresponding experimental energies, after subtracting the core contribution, in Fig. 6. It is quite clear from this figure that band 1 is reproduced by considering the prolate deformation, and for band 2 the oblate deformation reproduces the experimental energies. We also examined the alignment features of the observed band structures and the results of I versus rotational frequency, $\hbar\omega$ are presented in Fig. 7. It is evident from this figure that bands 1 and 2 are consistent with the characterisation of these as prolate and oblate band structures, respectively.

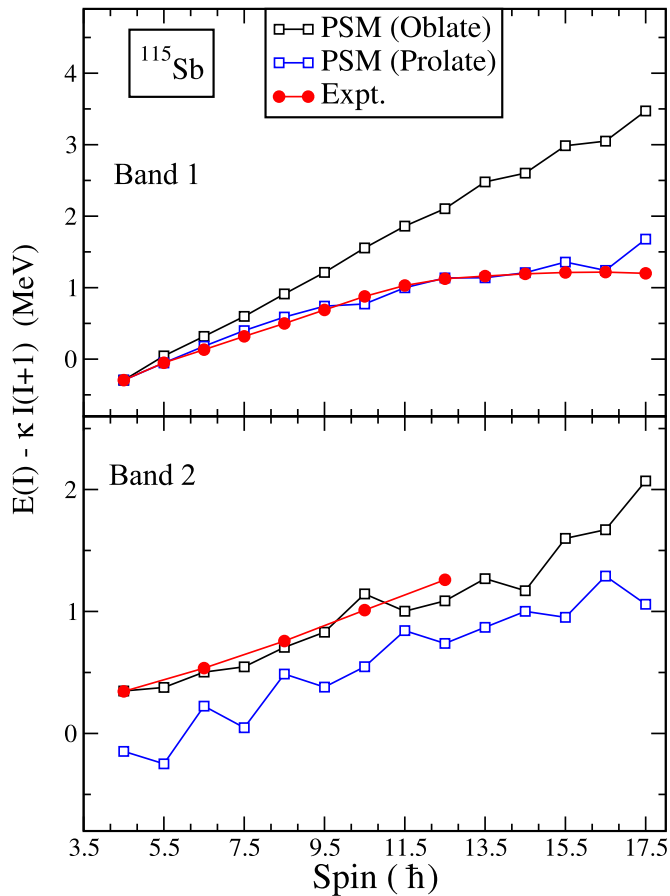


Fig. 6. PSM energies for the lowest two bands after configuration mixing are plotted along with the experimental data for ^{115}Sb .

To conclude, in this letter we presented an evidence of collective prolate-oblate shape coexistence in ^{115}Sb associated with the $g_{9/2}$ proton-hole configuration for the first time above $Z = 50$ shell closure. A new decoupled cascade of $E2$ transitions has been established above the $I^\pi = 9/2^+$ state at $E_{\text{level}} = 2019$ keV, based on the low- K $g_{9/2}$ orbital with oblate deformation. The experimental findings are found to be in good agreement with theoretical estimates from the PSM approach. Along with the previously reported high- K $g_{9/2}$ prolate deformed band, the present observation suggests that, in addition to its prolate driving nature, the $g_{9/2}$ orbital can also drive the nucleus towards an oblate shape. It has been also demonstrated that TRS calculations predict shape coexistence between prolate and oblate shapes at higher rotational frequency with prolate minimum being lower than the oblate one. For future studies, It would be interesting to search for such oblate deformed bands in odd- Z Iodine ($Z = 53$) and Cesium ($Z = 55$) isotopes (in which $g_{9/2}$ prolate structures are already known) to investigate such prolate-oblate shape driving effect of the $g_{9/2}$ orbital systematically in this region.

Declaration of competing interest

The authors declare the following financial interests/personal relationships which may be considered as potential competing interests:

Shabir Dar reports financial support was provided by University Grants Commission. S. Rajbanshi reports financial support was provided by University Grants Commission. S. Rajbanshi reports financial support was provided by Presidency University Kolkata. S. Chakraborty reports financial support was provided by Science and Engineering Research Board.

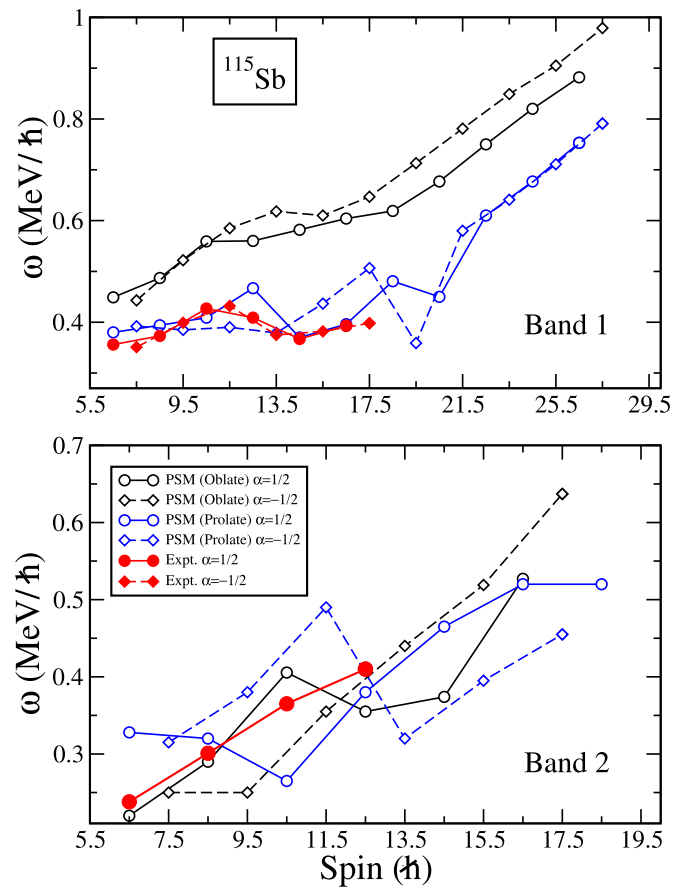


Fig. 7. The experimental and PSM angular frequencies versus the angular momentum for the ^{115}Sb nucleus.

Data availability

Data will be made available on request.

Acknowledgement

The authors would like to thank the members of VECC, SINP and UGC-DAE CSR (Kolkata centre) and the INGA collaboration for their support. The authors are also thankful to the operational staffs of the K-130 cyclotron at VECC for providing a good quality α beam for the present experiment. SD acknowledges the University Grants Commission (Sr. No. F.16-6(DEC. 2016)/2017(NET) and Ref. No.: 1490/(CSIR-UGC NET DEC. 2016). SN acknowledges the financial support received as research fellows from the Department of Atomic Energy (DAE), Government of India. SR acknowledges the financial assistance from the University Grants Commission Minor Research Project [Project No. PSW-249/15-16 (ERO)] and the FRPDF grant of Presidency University Kolkata, India. SC acknowledges the financial support received from the Science and Engineering Research Board (SERB, India) under National Post-Doctoral Fellowship (N-PDF) scheme *vide* reference no. PDF/2022/001829. The INGA facility is partially funded by Department of Science and Technology, Government of India (INGA Project No. IR/S2/PF-03/2003-I).

References

- [1] H. Morinaga, *Phys. Rev. C* 101 (1956) 254.
- [2] T. Engeland, *Nucl. Phys. A* 72 (1965) 68.
- [3] G.E. Brown, A.M. Green, *Nucl. Phys. A* 85 (1966) 87.
- [4] K. Heyde, et al., *Phys. Rep.* 102 (1983) 291.
- [5] J.L. Wood, et al., *Phys. Rep.* 215 (1992) 101.
- [6] K. Heyde, J. Wood, *Rev. Mod. Phys.* 83 (2011) 1467.

- [7] A.N. Andreyev, et al., *Nature* 405 (2000) 430.
- [8] A.V. Poelgeest, et al., *Nucl. Phys. A* 346 (1980) 70.
- [9] I. Thorslund, et al., *Phys. Rev. C* 52 (1995) R2839.
- [10] A. Sharma, et al., *Z. Phys. A* 354 (1996) 347.
- [11] A.K. Giagalis, et al., *Phys. Rev. Lett.* 35 (1975) 555.
- [12] R. Banik, et al., *Phys. Rev. C* 101 (2020) 014322.
- [13] R.E. Shroy, et al., *Phys. Rev. C* 19 (1979) 1324.
- [14] P. Van Nes, et al., *Nucl. Phys. A* 379 (1982) 35.
- [15] S. Vajda, et al., *Phys. Rev. C* 27 (1983) 2995.
- [16] G.J. Lane, et al., *Phys. Rev. C* 58 (1998) 127.
- [17] C.B. Moon, et al., *Nucl. Phys. A* 730 (2004) 3.
- [18] C.B. Moon, et al., *Nucl. Phys. A* 728 (2003) 350.
- [19] E.S. Paul, et al., *J. Phys. G, Nucl. Part. Phys.* 18 (1992) 837.
- [20] S. Juutinen, et al., *Z. Phys. A* 344 (1992) 223.
- [21] E.S. Paul, et al., *J. Phys. G, Nucl. Part. Phys.* 18 (1992) 971.
- [22] Y. Liang, et al., *Phys. Rev. C* 44 (1991) R578.
- [23] M.P. Waring, et al., *Phys. Rev. C* 49 (1994) 1878.
- [24] J. Timár, et al., *J. Phys. G, Nucl. Part. Phys.* 21 (1995) 783.
- [25] J. Simpson, et al., *Phys. Lett. B* 262 (1991) 388.
- [26] Y. Liang, et al., *Phys. Rev. Lett.* 64 (1990) 29.
- [27] K.K. Zheng, et al., *Phys. Lett. B* 822 (2021) 136645.
- [28] S. Das, et al., *Nucl. Instrum. Methods Phys. Res. A* 893 (2018) 138.
- [29] S.S. Nayak, G. Mukherjee, *IEEE Trans. Nucl. Sci.* 70 (2023) 2561.
- [30] A. Krämer-Flecken, et al., *Nucl. Instrum. Methods Phys. Res. A* 275 (1989) 333.
- [31] J. Rikowska, *Hyperfine Interact.* 26 (1985) 963.
- [32] C. Droste, et al., *Nucl. Instrum. Methods Phys. Res. A* 378 (1996) 518.
- [33] K. Starosta, et al., *Nucl. Instrum. Methods Phys. Res. A* 423 (1999) 16.
- [34] D.C. Radford, *Nucl. Instrum. Methods Phys. Res. A* 361 (1995) 297.
- [35] S. Dar, et al., *Nucl. Phys. A* 1019 (2022) 122382.
- [36] R.S. Chakravarthy, et al., *Phys. Rev. C* 54 (1996) 2319.
- [37] B.E. Chi, *Nucl. Phys.* 83 (1966) 97.
- [38] D.R. LaFosse, et al., *Phys. Rev. C* 56 (1997) 760.
- [39] D.R. LaFosse, et al., *Phys. Rev. Lett.* 69 (1992) 1332.
- [40] D.B. Fossan, et al., *Phys. Rev. C* 15 (1977) 1732.
- [41] Y. Liang, et al., *Phys. Rev. C* 45 (1992) 1041.
- [42] S. Dar, et al., *Proc. DAE Symp. on Nucl. Phys.* 65 (2021) 52.
- [43] W. Nazarewicz, et al., *Nucl. Phys. A* 435 (1985) 397.
- [44] W. Nazarewicz, et al., *Nucl. Phys. A* 512 (1990) 61.
- [45] G. Mukherjee, et al., *Nucl. Phys. A* 829 (2009) 137.
- [46] S.S. Nayak, G. Mukherjee, *Nucl. Phys. A* 1023 (2022) 122449.
- [47] S.S. Nayak, G. Mukherjee, *Int. J. Mod. Phys. E* 31 (2022) 2250048.
- [48] S. Nandi, et al., *Phys. Rev. C* 99 (2019) 054312.
- [49] K. Hara, Y. Sun, *J. Mod. Phys. E* 4 (1995) 637.
- [50] K. Hara, Y. Sun, *Nucl. Phys. A* 531 (1991) 221.
- [51] R. Palit, et al., *Nucl. Phys. A* 686 (2001) 141.
- [52] Y. Sun, J.A. Sheikh, *Phys. Rev. C* 64 (2001) 031302.
- [53] Y. Sun, J.L. Egido, *Nucl. Phys. A* 580 (1994) 1.
- [54] Y. Sun, et al., *Phys. Rev. C* 62 (2000) 021601.
- [55] K. Hara, S. Iwasaki, *Nucl. Phys. A* 332 (1979) 61.
- [56] K. Hara, S. Iwasaki, *Nucl. Phys. A* 348 (1980) 200.
- [57] S.G. Nilsson, et al., *Nucl. Phys. A* 131 (1969) 1.
- [58] I.L. Lamm, *Nucl. Phys. A* 125 (1969) 504.
- [59] P. Ring, P. Schuck, *The Nuclear Many-Body Problem*, Springer-Verlag, New York, 1980.